RESEARCH ARTICLE | JANUARY 05 2024

Ultra-broadband sound absorption in a compact multi-chamber micro-perforated panel absorber with varying depths

Jiayu Wang ; Gareth J. Bennett

AIP Advances 14, 015009 (2024)
https://doi.org/10.1063/5.0187328

Ultra-broadband sound absorption in a compact multi-chamber micro-perforated panel absorber with varying depths

Cite as: AIP Advances 14, 015009 (2024); doi: 10.1063/5.0187328
Submitted: 14 November 2023 • Accepted: 9 December 2023 •
Published Online: 5 January 2024

Jiayu Wang[a] and Gareth J. Bennett[a]

AFFILIATIONS

Department of Mechanical, Manufacturing and Biomedical Engineering, Trinity College Dublin, the University of Dublin, D02 PN40 Dublin, Ireland

[a]Authors to whom correspondence should be addressed: wangj12@tcd.ie and gareth.bennett@tcd.ie

ABSTRACT

This study presents an enhanced multi-chamber micro-perforated panel absorber (MC-MPPA) with varying sub-chamber depths, offering ultra-broadband low-frequency sound absorption. Traditional micro-perforated panel absorbers are constrained by a limited bandwidth, necessitating impossibly small perforations for optimal low-frequency absorption. Our innovative design addresses these constraints with a lightweight, compact panel structure that uses varied chamber depths and unique porosities. Using the two-point impedance method from graph theory, an MC-MPPA was modeled and optimized. Notably, our MC-MPPA test pieces achieved impressive sound absorption coefficients experimentally of over 0.8 in the whole frequency ranges of [397–1000] and [698–1895] Hz. The absorber's thickness is a mere 47 mm, equivalent to 1/18.2 and 1/10.5 of the sound wavelength at the minimum operational frequency, respectively. Theoretically, with a maximum sub-chamber depth of just 20 mm, average absorption coefficient values of 0.6780 and 0.6483 were observed in [200–3000] and [200–4000] Hz ranges, respectively. Our optimization algorithm permits the definition of practical geometric parameters, promising substantial industrial benefits. The results have been validated theoretically, numerically, and experimentally.

I. INTRODUCTION

Micro-perforated panel absorbers (MPPAs)[1–3] have become an increasingly popular solution for sound absorption in recent years. MPPAs are absorbers whose panels are perforated with micro-sized holes, typically less than 1 mm in diameter, and whose porosity is typically most effective in the range [0%–5%].[4–6] The combination of micro-perforations with an air-backing cavity creates a compressibility effect resonant system that is highly efficient at absorbing acoustic energy. However, the conventional design of MPPAs exhibits inadequate absorption capability in the low-frequency range, as well as a typically narrow absorption bandwidth, particularly in shallow applications where the space for acoustic treatment is constrained. Therefore, the development of a light, compact micro-perforated panel structure that can effectively absorb low-frequency and broadband sound continues to present an intractable challenge.

To date, extensive efforts have been expended in the pursuit of the development of a lightweight micro-perforated panel absorber with exceptional acoustic performance. Authors in one research laboratory[7–9] introduced an innovative sound absorber that exploits the viscothermal dissipative traits of the micro-perforated plate (MPP) and effectively reduces its frequency response by integrating decorated membrane resonators. Experimental results demonstrate that this compact absorber can achieve low-frequency broadband sound absorption at deep, subwavelength thicknesses. Carbajo *et al.*[5] and Wang and Bennett[6] explored how micro-perforated partitions can effectively broaden the sound absorption bandwidth of MPPAs. Kim and Yoon[10] discovered that an MPP with multiple-sized holes and a porous separating partition in a MPPA can result in a wider sound absorption bandwidth when compared to a conventional rigid partition MPPA. Wang *et al.*[4] proposed a novel MPPA incorporating a trapezoidal cavity that facilitates superior vibroacoustic coupling between the micro-perforated panel and

the cavity, ultimately broadening the sound absorption bandwidth of the MPPA. Yang, Choy, and Li[11] conducted a study on the sound absorption capabilities of a wavy MPPA, ultimately devising a compact wavy MPPA that achieves a high random sound absorption coefficient (SAC) through an optimization methodology. Bravo *et al.*[12–14] conducted a study on the effect of panel vibrations on the acoustic properties of thin MPPAs and subsequently improved the sound absorption performance of these MPPAs using the impedance boundary optimization method. Wang and Huang[15] examined the sound absorption properties of a compound MPPA array, comprised of three MPPAs arranged in parallel with varying cavity depths. Their results indicate that the MPPA array requires a lower acoustic resistance for effective sound absorption compared to a single MPPA. Drawing inspiration from the traditional perforated panel concept, Li, Yu, and Zhai[16] introduced a novel sound absorber based on a microlattice, exhibiting an average experimental SAC of 0.77 across a broad frequency range spanning from 1000 to 6300 Hz. Furthermore, this innovative design offers additional multifunctionality in terms of impact resistance.

Research progress in micro-perforated sound absorbers is greatly influenced by the evolution of process and manufacturing technologies.[17,18] The advancement in these technologies can result in the development of more advanced and efficient MPPAs.[17,19–21] Despite the substantial advancements achieved in the past two decades, there remain limitations in their scope and nature. As early as 1998, Maa[3] postulated that the attainment of broadband sound absorption in a single-layer micro-perforated sound absorber could be realized through a reduction in the perforation diameter (below 0.1 mm) and an increase in the perforation ratio.[6,22] In a prior investigation,[6] the impact of pore size and perforation rate on the sound absorption characteristics of an MC-MPPA was investigated. The analytical results indicated that when the noise of interest was white noise, there was a strong agreement between the theory put forth by Maa[3] and the observed increase in the sound absorption bandwidth with decreasing perforation size. However, the creation of perforations of such diminutive size, particularly in instances where the perforation ratio is substantial, presents a huge challenge and results in a subpar economic efficiency for traditional processing techniques, such as machine punching, and for additive manufacturing technologies, such as 3D printing. Therefore, the design and fabrication of an MPPA with an excellent acoustic performance within the confines of current common processing and manufacturing technologies constitutes a noteworthy undertaking, with far-reaching practical applications in industry and a significant economic value.

In this research, a novel and robust absorber with sub-chambers of varying depth and porosity is presented. Its design and optimization is facilitated by the introduction and original application of the TpIM, which enables the modeling of a technology of such complexity. The introduction of the TpIM to acoustic metamaterial modeling is a milestone as the ubiquitous equivalent circuit model (ECM) method based on electro-acoustic analogies can only represent very basic circuits and so has been an obstacle to innovative development. The current work has the following objectives: (1) To develop and optimize a multi-chamber MPPA where each sub-chamber can have unique porosity both on the faceplate and on internal partitions as well as unique depth. (2) To achieve ultra-broadband sound absorption with this novel MC-MPPA. (3) To identify which parameters are most critical to control during production to maintain optimal absorption characteristics through a sensitivity analysis. (4) To design and fabricate a compact MC-MPPA whose geometric details are achievable with reasonable current processing and manufacturing technologies. (5) To validate the compact MC-MPPA design numerically and experimentally.

II. DESIGN AND THE TWO-POINT IMPEDANCE METHOD (TPIM)

As illustrated in Fig. 1, a rectangular MC-MPPA is characterized by adjacent panels with differing porosities and has varying depths of its sub-chambers. The investigated MC-MPPA structure is divided into nine chambers in a 3×3 configuration, where each chamber can possess unique depths and is separated by micro-perforated adjacent panels. The dimensions of the MC-MPPA are denoted by length L and width W. The thickness of the *top* MPPs in the MC-MPPA is symbolized as τ_t, whereas the thickness of the *internal* micro-perforated adjacent panels is represented by τ_i. The total height, H, of the MC-MPPA is obtained by summing τ_t and the maximum sub-chamber depth, $D_{\max}$. Throughout this paper, the overall MC-MPPA depth specifically refers to the deepest sub-chamber's depth, $D_{\max}$. The key parameters of the investigated MC-MPPA are outlined in Table I. We keep the perforation number n as a variable as its control is necessary to prevent an unreasonably high value inhibiting manufacture. In addition, both τ_t and τ_i are fixed with predefined thicknesses corresponding to off-the-shelf availability. While both of these parameters could be allowed to vary relative to each other and as a function of sub-chamber in the optimization routine, it was decided that a constant plate thickness from chamber to chamber would be much more practical for manufacture/assembly.

In this study, the two-point impedance method (TpIM) is introduced and applied to determine the impedance of the MC-MPPA. The typically used equivalent circuit model (ECM) method uses electrical circuit analogies and can be used to characterize the operational parameters of an acoustic system but only for very simple circuits. The ECM usually uses Δ–Y and Y–Δ transforms to simplify the circuit to estimate acoustic impedance.[5] However, as the complexity of the acoustic system increases, the ECM becomes unmanageable.[8] For this reason, we have developed a graph-theory approach, based on the two-point impedance theory proposed by

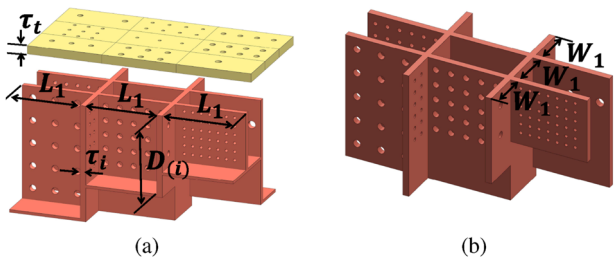

FIG. 1. Schematic of the enhanced MC-MPPA. (a) Structural arrangement of the MC-MPPA. (b) Micro-perforated adjoining panels of the MC-MPPA with varying sub-chamber depths. Solid bases and top MPP not shown for clarity.

TABLE I. Parameters that define the acoustic behavior of the MC-MPPA under study.

Location of MPPs	Symbol of MPPs	Panel thickness	Perforation diameter	Perforation porosity	Perforation number	Sub-chamber depths
Top surface	$MPP_{t(1)}$	τ_t	$d_{t(1)}$	$\varphi_{t(1)}$	$n_{t(1)}$	$D_{(1)}$
	$MPP_{t(2)}$		$d_{t(2)}$	$\varphi_{t(2)}$	$n_{t(2)}$	$D_{(2)}$
	$MPP_{t(3)}$		$d_{t(3)}$	$\varphi_{t(3)}$	$n_{t(3)}$	$D_{(3)}$
	⋮		⋮	⋮	⋮	⋮
	$MPP_{t(9)}$		$d_{t(9)}$	$\varphi_{t(9)}$	$n_{t(9)}$	$D_{(9)}$
Internal walls	$MPP_{i(1)}$	τ_i	$d_{i(1)}$	$\varphi_{i(1)}$	$n_{i(1)}$	
	$MPP_{i(2)}$		$d_{i(2)}$	$\varphi_{i(2)}$	$n_{i(2)}$	
	$MPP_{i(3)}$		$d_{i(3)}$	$\varphi_{i(3)}$	$n_{i(3)}$	
	⋮		⋮	⋮	⋮	
	$MPP_{i(12)}$		$d_{i(12)}$	$\varphi_{i((12)}$	$n_{i(12)}$	

Tzeng and Wu[23] previously used in the domain of electronics, but used here instead to estimate acoustic impedance. Figure S1 of the supplementary material shows the investigated MC-MPPA from Figs. 1(a) and 1(b) represented schematically as a bi-pyramidal molecular structure. The objective here is to calculate the impedance of the overall system, i.e., between nodes 1 and 11 using a matrix approach.

The primary objective of employing the TpIM in our MC-MPPA technology is to develop an analytical model that allows the performance of the MC-MPPA to be *optimized* to calculate the maximum SAC possible within a specified set of parameters. In our case, we can establish an optimization cost function that characterizes the total SAC within a specified frequency range:

$$C_\alpha = 10\log_{10}(1 - c_\alpha). \tag{1}$$

Here, c_α represents the comprehensive SAC, proportionally balanced by the sound spectrum of the intended noise source,

$$c_\alpha = \frac{\left(\sum_{\omega_1}^{\omega_2} \alpha(\omega) G_{xx}(\omega)\right)}{\left(\sum_{\omega_1}^{\omega_2} G_{xx}(\omega)\right)}. \tag{2}$$

Here, ω_1 is equivalent to $2\pi f_1$ and ω_2 corresponds to $2\pi f_2$, where f_1 and f_2 represent the lower and upper bounds of the frequency range under consideration. The SAC, denoted as $\alpha(\omega)$, is determined following the TpIM procedure in the supplementary material with the intended sound spectrum characterized by an auto-spectral density function, $G_{xx}(\omega)$. In this research, the target noise is white noise, $G_{xx}(\omega) \equiv 1$. We employed the Sequential Quadratic Programming (SQP) optimization technique to minimize the cost function.

Full details of the acoustic modeling and optimization procedures for the MC-MPPA employing the two-point impedance method can be found in the supplementary material. Detailed accounts of the experimental and numerical sound absorption procedures conducted on the MC-MPPA and used for validation are also provided in the supplementary material.

Two MC-MPPA experimental samples, which were optimized for frequencies of [20–1000] and [20–2000] Hz, were fabricated, of which the latter is shown in detail in Fig. 2. Both the core (air cavities and perforated adjoining panels) and the top MPPs were 3D printed with a Masked Stereolithography Apparatus (MSLA). The maximum depth of the sub-chamber air-cavity in both samples was 45 mm, and the total thickness of each technology was 47 mm, including the thickness of τ_t. Masked stereolithography is a 3D printing process, which uses photopolymer resins that can be cured by UV light at a wavelength of 405 nm. The optimized geometric parameters of the experimental Test Pieces 1000 and 2000 can be found in Tables S6–S7 of the supplementary material.

III. RESULTS

Figure 3 displays the analytical SAC curves of MC-MPPAs that have been optimized for four different frequency ranges: [20–1000], [20–2000], [20–3000], and [20–4000] Hz. The geometric parameters of the MC-MPPA that correspond to each of the absorption curves in Fig. 3 are provided in Tables S2–S5 of the supplementary material. Furthermore, Table II provides the specific values of c_α for Fig. 3 in the four different frequency ranges as a function of D_{max}. It is clear that the c_α value is dependent on the frequency range chosen for evaluation and that values of above 0.8 and even 0.9 over a wide frequency range can be attained through a judicious choice of the frequency limits of optimization.

Figure 4 shows a comparison of the analytical results to numerical results, which were calculated using COMSOL, in the same frequency ranges, of the MC-MPPAs with varying overall absorber

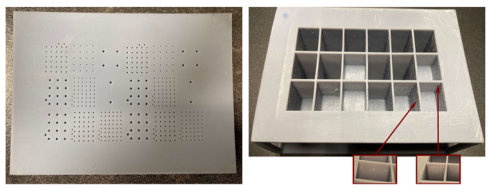

(a) (b)

FIG. 2. Photograph of the MC-MPPA test samples. (a) The top MPP and the core are both 3D printed. (b) The sub-chambers of the core have perforated adjacent panels of differing parameters, and the sub-chamber depths differ from each other.

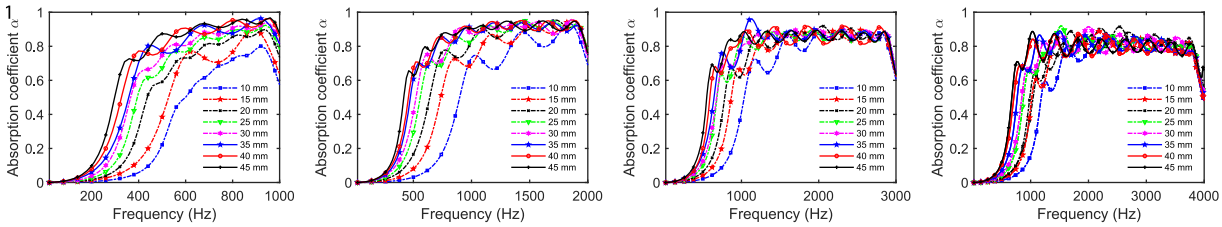

(a) 20–1000 Hz (b) 20–2000 Hz (c) 20–3000 Hz (d) 20–4000 Hz

FIG. 3. Analytical SACs of the optimized MC-MPPA as a function of core depth and optimized frequency range.

TABLE II. Overall SACs of the MC-MPPA in four different frequency ranges (data correspond to the SACs curves in Fig. 3).

(200–1000) Hz		(200–2000) Hz		(200–3000) Hz		(200–4000) Hz	
D_{max} (mm)	c_α	D_{max} (mm)	c_α	D_{max} (mm)	c_α	D_{max} (mm)	c_α
10	0.4097	10	0.5200	10	0.5905	10	0.5881
15	0.5000	15	0.6153	15	0.6479	15	0.6249
20	0.5818	20	0.6772	20	0.6780	20	0.6483
25	0.6393	25	0.7138	25	0.7008	25	0.6625
30	0.6855	30	0.7340	30	0.7158	30	0.6727
35	0.7163	35	0.7541	35	0.7261	35	0.6821
40	0.7527	40	0.7665	40	0.7305	40	0.6874
45	0.7834	45	0.7812	45	0.7424	45	0.6984

thickness across different frequency ranges. These figures were generated to investigate the relationship between the absorber thickness and sound absorption performance of the MC-MPPA for various frequencies ranges. The numerical results presented in these figures serve to validate the analytical results depicted in Fig. 3 and increase confidence in the novel TpIM approach to analytical modeling and the optimization algorithm.

Investigating the sensitivity of broadband absorption performance to various types of parameters becomes crucial when considering uncertainties in manufacturing parameters. Through the analysis of the theoretical model, it is possible to determine which parameters significantly impact the broadband absorption performance and which parameters have a relatively minor effect. Figure 5 presents an analysis of the sensitivity of the MC-MPPA's geometric parameters. This analysis aims to derive general principles from the theoretical model that can inform optimization and practical manufacturing processes, thus ensuring the stability and reliability of the broadband absorption performance.

In order to provide experimental validation, Figs. 6(a) and 6(c) depict the analytical, numerical, and experimental SACs of the Test Piece 1000 and Test Piece 2000 MC-MPPA samples. These figures provide a comprehensive comparison between the expected and actual SACs of the MC-MPPA in these frequency ranges. The acoustic resistance and reactance of Test Piece 1000 and Test Piece 2000 MC-MPPA samples, both numerical and experimental, are plotted in Figs. 6(b) and 6(d).

To emphasize the compactness of the MC-MPPA design, illustrated by the ratio of the structure's thickness to its minimum operational wavelength, Fig. 7 presents a comparative study. This study underscores the MC-MPPA's effective performance, especially regarding its absorption bandwidth and efficiency at deep-subwavelength scales.

IV. DISCUSSIONS

A. Absorption response of the MC-MPPA

Regarding the acoustic response of the MC-MPPA, the results demonstrate ultra-broadband sound absorption characteristics when all parameters of each chamber are allowed to vary independently. Figure 6(a) shows that an overall SAC over 0.8 can be achieved experimentally by the MC-MPPA at a maximum sub-chamber depth of only 45 mm in the frequency range of 276–1000 Hz, while Fig. 6(c) demonstrates that the same SAC value can be achieved at a maximum sub-chamber depth of 45 mm in the frequency range of 325–2000 Hz. Additionally, for higher frequencies, as presented in Fig. 3 and Table II, the overall SAC of MC-MPPA at a maximum sub-chamber depth of 45 mm is 0.7424 and 0.6984 at frequency ranges of [200–3000] and [200–4000] Hz, respectively. Notably, even at a maximum sub-chamber depth of only 20 mm, the MC-MPPA achieves an overall SAC of 0.6780 and 0.6483 in the frequency ranges of [200–3000] and [200–4000] Hz, respectively.

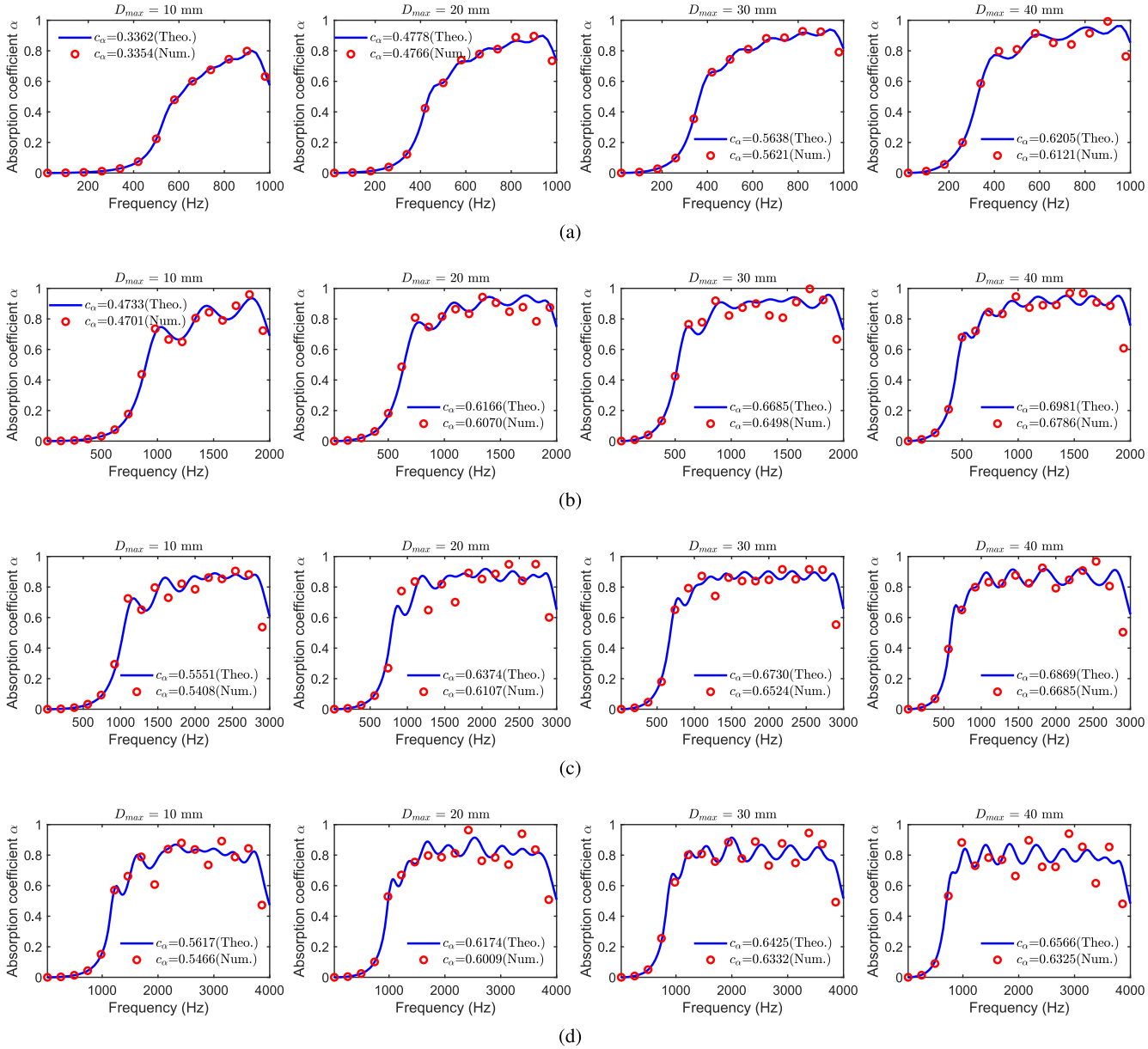

FIG. 4. Analytical and numerical SACs of MC-MPPAs with different overall absorber thicknesses in different frequency ranges. (a) [20–1000] Hz. (b) [20–2000] Hz. (c) [20–3000] Hz. (d) [20–4000] Hz.

Regarding the "compact" acoustic performance of the MC-MPPA, as illustrated in Figs. 6(a) and 6(c), the experimental SACs of Test Piece 1000 exceed 0.8 within the frequency range of 397–1000 Hz. Remarkably, the absorber's thickness is a mere 47 mm, equivalent to 1/18.2 of the sound wavelength at the minimum operational frequency. Similarly, the SACs of Test Piece 2000 surpass 0.8 in the 698–2000 Hz frequency range, with the absorber maintaining the same thickness, equating to 1/10.5 of the sound wavelength at its minimum operational frequency.

The MC-MPPA's acoustic absorption capabilities can also be explained by its acoustic reactance and resistance, as shown in Figs. 6(b) and 6(c). An ideal impedance match requires the acoustic reactance to be zero and the acoustic resistance to be one, achieved simultaneously. Analysis of the numerical and experimental acoustic reactance and resistance in Figs. 6(b) and 6(c) reveals that the numerical and experimental results align closely, a finding previously established. Significantly, within the frequency range where SAC exceeds 0.8, Figs. 6(a) and 6(b) indicate that the acoustic

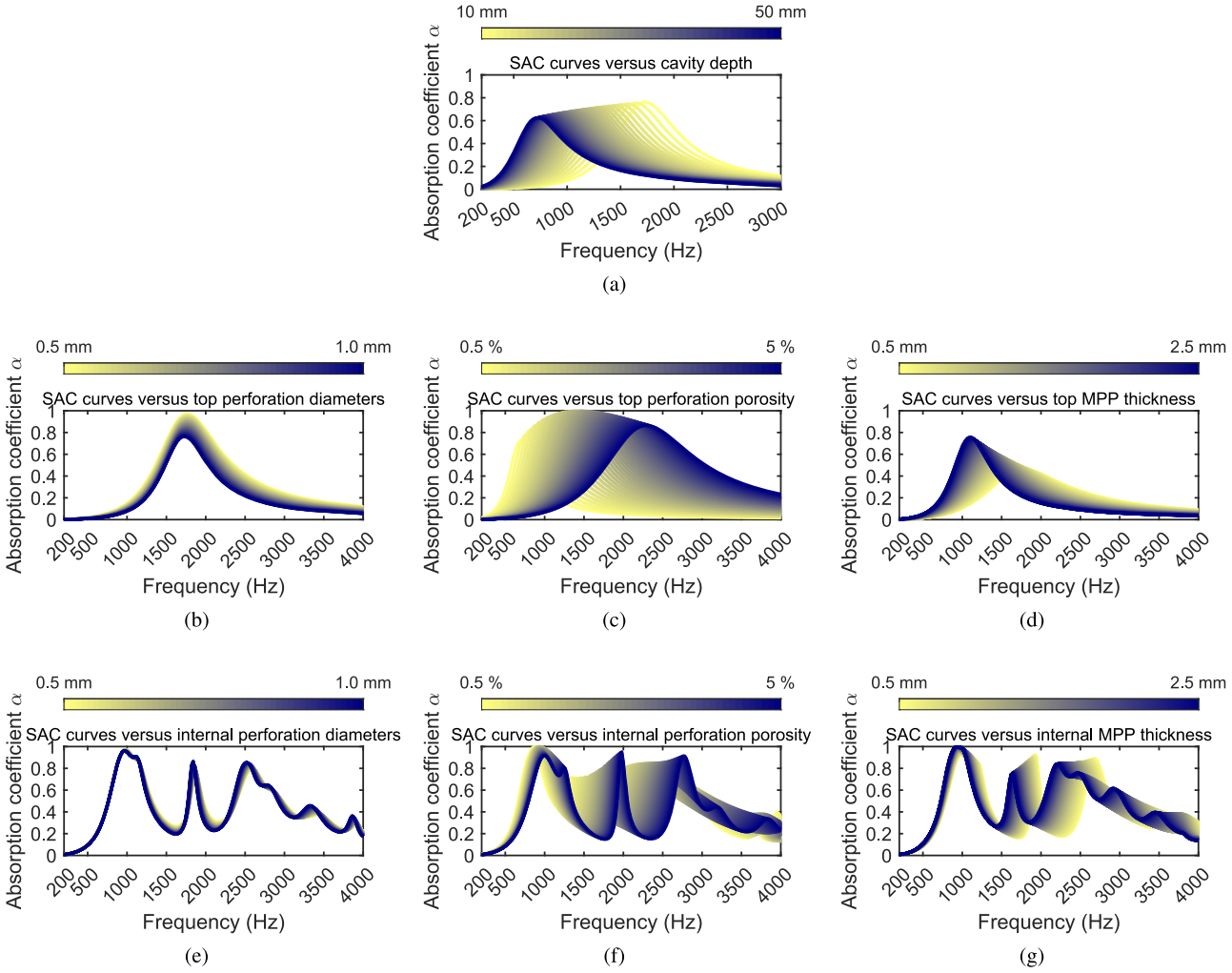

FIG. 5. Sensitivity analysis of MC-MPPA's geometric parameters. (a) Curve's color gets darker as the depth increases from 10 to 50 mm. [(b) and (e)] Curve's color gets darker as the perforation diameter increases from 0.5 to 1.0 mm. [(c) and (f)] Curve's color gets darker as the perforation porosity increases from 0.5% to 5.0%. [(d) and (g)] Curve's color gets darker as the thickness increases from 0.5 to 2.5 mm.

reactance approaches zero and the acoustic resistance nears one. This pattern is also observed in Figs. 6(c) and 6(d). Specifically, for Test Piece 2000, the experimental data at ~1400 Hz show acoustic reactance approximately zero and acoustic resistance close to one, aligning with its experimental absorption curve at the same frequency, where SAC nearly reaches one.

B. Impact of the air cavity depth in sub-chambers

As can be seen from Fig. 3 and Table II, an increase in the *maximum* sub-chamber depth, D_{max}, corresponds to an enhancement in the SAC of the MC-MPPA. In this research, it has been observed that fixing the sub-chamber depths to a common value limits the operating frequency of the MC-MPPA. However, as illustrated in Fig. 3 and Table II, allowing the depths to vary from one sub-chamber to another effectively broadens the operating frequency range from [200–2 000] to [200–4 000] Hz. Upon further investigation, as detailed in the supplementary material, it is observed that when the optimized frequency is confined to 20–1000 Hz, the depths of individual sub-cavities tend to remain consistent. However, as the upper limit of the optimized frequency increases, the difference in depth among sub-cavities within the same MC-MPPA becomes more pronounced. This observation further corroborates the conclusion from an alternative perspective.

C. Sensitivity analysis of MC-MPPA's geometric parameters

Given the precision required in MC-MPPA manufacturing, even slight deviations in geometric parameters can significantly impact performance. A sensitivity analysis is essential to identifying

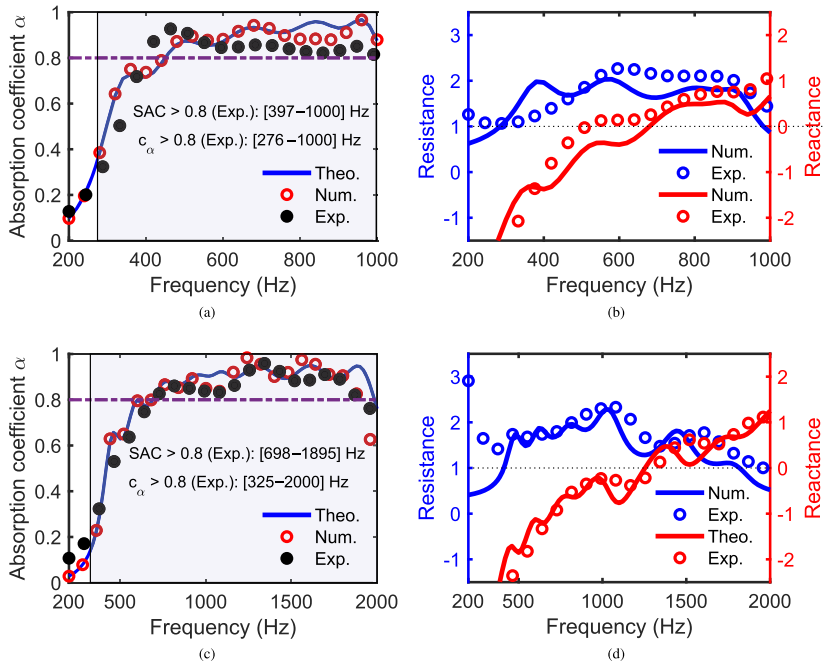

FIG. 6. (a) Analytical, numerical, and experimental SACs of Test Piece 1000. (b) Numerical and experimental acoustic resistance and reactance of Test Piece 1000. (c) Analytical, numerical, and experimental SACs of Test Piece 2000. (d) Numerical and experimental acoustic resistance and reactance of Test Piece 2000.

which parameters are most critical to control during production to maintain optimal absorption characteristics.

We analyze the sensitivity of seven key geometric parameters: chamber depth, top MPP's perforation diameters, top MPP's perforation porosity, top MPP's perforation thickness, internal MPP's perforation diameters, internal MPP's perforation porosity, and internal MPP's perforation thickness. The results are plotted in Fig. 5. Each of these parameters plays a crucial role in determining the acoustic impedance and, consequently, the absorption performance of the MC-MPPA. In this analysis, the ranges of parameters have been chosen under the current common processing and manufacturing technologies. Details of the sensitivity analysis of MC-MPPA's geometric parameters can be found in Sec. S5 of the supplementary material.

The analysis demonstrates that the broadband absorption performance exhibits significant sensitivity to the chamber depth and the porosity of the top and internal MPPs, while showing moderate sensitivity to the panel thickness. Conversely, alterations in the diameters of the top and internal MPPs' perforations have a negligible impact. This evidence indicates that stricter regulation of chamber depth, perforation porosity, and MPP thickness during production can lead to substantial enhancements in performance consistency. These findings offer critical guidance for optimizing the MC-MPPA and its manufacturing process in future research and can explain the differences between the experimental and analytical/numerical results.

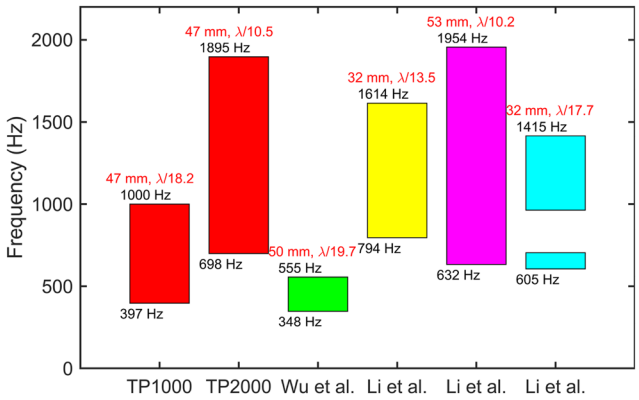

FIG. 7. Comparison of sound absorption bandwidth (SAC >0.8) among MC-MPPAs and other compact broadband MPP-type sound absorbers.

D. Numerical and experimental validation

Regarding the numerical validation, Fig. 4 presents a comparison between the analytical and numerical SACs of MC-MPPAs for varying overall absorber thicknesses across the four distinct frequency ranges. Generally, the numerical simulations agree well with the analytical results. Upon closer examination, minor discrepancies are observed with increasing depth and frequency. These marginal discrepancies may be explained by a violation of the lumped element assumption and the possibility that the spacing between the perforations is not negligible. A more exhaustive exploration of

these phenomena will ensue in subsequent studies. Regarding the experimental validation, as illustrated in Fig. 6, the experimental results demonstrate a high degree of agreement with both the analytical values and the numerical simulations and demonstrate that the design is more than just conceptual but is realizable.

E. Analysis of the processing and manufacturing challenges associated with the MC-MPPA under investigation

Generating numerous micro-holes (with diameters smaller than 0.3 mm) in a thin sheet presents a substantial challenge for both 3D printers and Computer Numerical Control (CNC) milling machines. Even when successfully produced, the process requires significant time and specialized equipment cost. Consequently, large-scale engineering applications employing micro-perforated plates with diameters less than 0.3 mm are limited by their economic efficiency. In principle, an increase in diameter and a decrease in the number of micro-holes machined in a thin plate result in reduced requirements for the machining and manufacturing process, decreased production costs, and enhanced potential for large-scale industrial applications.

In this study, we took into account not only the SAC performance of the MC-MPPA but also the processing and manufacturing challenges associated with the designed MC-MPPA. Consequently, we controlled the diameter of the micro-holes to be within the range of 0.5–1.0 mm and the porosity to be between 0% and 5%. In addition, the plate thicknesses were fixed at 1 and 2 mm. This design can undoubtedly be easily printed or machined by the vast majority of 3D printers and CNC machines. Examining the geometric parameters (listed in Tables S6 and S7 of the supplementary material) of our two MC-MPPA test pieces, Test Piece 1000 and Test Piece 2000, reveals that the smallest micro-hole diameter is 0.5 mm and the largest number of holes is 183, which are reasonable quantities.

F. Comparative analysis

Figure 7 presents a comparison of the sound absorption bandwidth (SAC >0.8) between the MC-MPPA and other compact broadband MPP-type sound absorbers. In this figure, the red bars represent the MC-MPPAs under investigation, namely Test Piece 1000 (TP1000) and Test Piece 2000 (TP2000), with data sourced from Figs. 6(a) and 6(c). The green bar illustrates the hybrid sound absorber described by Wu *et al.*,[24] which combines a MPP and coiled-up Fabry–Pérot channels. The yellow bar depicts the MPPA with an integrated Helmholtz resonator, as explored in Li *et al.*[25] The magenta bar represents the single-layer MPPA from Li *et al.*,[25] while the cyan bar corresponds to the double-layer MPPA, also from Li *et al.*[25] It is important to note that all the data compared are experimental. The sound acoustic performance of the MC-MPPA is notably high, particularly from the aspects of absorption bandwidth and efficiency at deep-subwavelength levels. This efficiency is distinctly marked by the proportion of the structure's thickness relative to its minimum operational wavelength.

V. CONCLUSION

This research concentrates on exploring the acoustic properties of an MC-MPPA while varying the depths of sub-chambers. The acoustic properties of our designed MC-MPPA have been evaluated, taking into account the limitations of the current processing and manufacturing technologies. The investigation led to the following findings:

1. A compact MC-MPPA can demonstrate ultra-broadband sound absorption capabilities. The experimental results from MC-MPPAs, with a thickness of only 47 mm, exhibit an overall average SAC exceeding 0.8 within the frequency ranges of [276–1000] and [325–2000] Hz. Theoretically, even with a maximum sub-chamber depth of just 20 mm, the MC-MPPA attains overall SACs of 0.6780 and 0.6483 in the frequency ranges of [200–3000] and [200–4000] Hz, respectively.
2. The experimental SACs of Test Piece 1000 exceed 0.8 within the whole frequency range of 397–1000 Hz. Remarkably, the absorber's thickness is a mere 47 mm, equivalent to 1/18.2 of the sound wavelength at the minimum operational frequency.
3. The variable sub-chamber depth of the MC-MPPA considerably broadens the sound absorption bandwidth. Varying sub-chamber depths effectively extends the operating frequency range from [200–2000] to [200–4000] Hz and simultaneously improves performance.
4. Sensitivity analyses show that the absorption performance of MC-MPPA is predominantly influenced by several key factors: the chamber depth, the porosity of the top and internal micro-perforated panels (MPPs), and the thickness of their perforations. Consequently, these parameters warrant meticulous regulation throughout the design and fabrication process to guarantee uniform performance.
5. The design and fabrication of a compact MC-MPPA exhibiting an exceptional acoustic performance is achievable through the current common processing and manufacturing technologies, providing substantial practical applications and an economic value within the industry.
6. While a 3×3 chamber MC-MPPA was examined, other geometries can be modeled. Similarly, the depths and frequency ranges were chosen as examples only of what is possible.
7. As every optimized curve has a frequency dependent ramp-up and ramp-down in the absorption coefficient, designs can be made such that the high level absorption plateau spans the frequency range of interest. This will result in even high average absorption values.

SUPPLEMENTARY MATERIAL

For detailed information on the acoustic modeling, optimization procedures, sensitivity analyses, and sound absorption measurements of the MC-MPPA, along with its geometric parameters, refer to the supplementary material.

ACKNOWLEDGMENTS

This project received funding from the European Union's Horizon 2020 research and innovation program under grant Agreement No. 860538 for the project INVENTOR. Jiayu Wang was supported under the China Scholarship Council (CSC) – Trinity College Dublin Joint Scholarship Programme.

AUTHOR DECLARATIONS

Conflict of Interest

The authors have no conflicts to disclose.

Author Contributions

Jiayu Wang: Conceptualization (equal); Data curation (lead); Investigation (lead); Methodology (equal); Software (equal); Visualization (lead); Writing – original draft (equal); Writing – review & editing (equal). **Gareth J. Bennett**: Conceptualization (equal); Methodology (equal); Resources (lead); Software (equal); Supervision (lead); Writing – original draft (lead); Writing – review & editing (equal).

DATA AVAILABILITY

The data that support the findings of this study are available from the corresponding authors upon reasonable request.

REFERENCES

[1]D.-Y. Maa, "Theory and design of microperforated panel sound-absorbing constructions," Sci. Sin. **18**, 55–71 (1975).
[2]D.-Y. Maa, "Microperforated-panel wideband absorbers," Noise Control Eng. J. **29**, 77–84 (1987).
[3]D.-Y. Maa, "Potential of microperforated panel absorber," J. Acoust. Soc. Am. **104**, 2861–2866 (1998).
[4]C. Wang, L. Cheng, J. Pan, and G. Yu, "Sound absorption of a micro-perforated panel backed by an irregular-shaped cavity," J. Acoust. Soc. Am. **127**, 238–246 (2010).
[5]J. Carbajo, J. Ramis, L. Godinho, and P. Amado-Mendes, "Perforated panel absorbers with micro-perforated partitions," Appl. Acoust. **149**, 108–113 (2019).
[6]J. Wang and G. J. Bennett, "Multi-chamber micro-perforated panel absorbers optimised for high amplitude broadband absorption using a two-point impedance method," J. Sound Vib. **547**, 117527 (2023).
[7]A. McKay, I. Davis, J. Killeen, and G. J. Bennett, "SeMSA: A compact super absorber optimised for broadband, low-frequency noise attenuation," Sci. Rep. **10**, 17967 (2020).
[8]I. Davis, A. McKay, and G. J. Bennett, "A graph-theory approach to optimisation of an acoustic absorber targeting a specific noise spectrum that approaches the causal optimum minimum depth," J. Sound Vib. **505**, 116135 (2021).
[9]J. Killeen, I. Davis, J. Wang, and G. J. Bennett, "Fan-noise reduction of data centre telecommunications' server racks, with an acoustic metamaterial broadband, low-frequency sound-absorbing liner," Appl. Acoust. **203**, 109229 (2023).
[10]K. H. Kim and G. H. Yoon, "Absorption performance optimization of perforated plate using multiple-sized holes and a porous separating partition," Appl. Acoust. **120**, 21–33 (2017).
[11]W. Yang, Y. Choy, and Y. Li, "Acoustical performance of a wavy micro-perforated panel absorber," Mech. Syst. Signal Process. **185**, 109766 (2023).
[12]T. Bravo, C. Maury, and C. Pinhède, "Vibroacoustic properties of thin micro-perforated panel absorbers," J. Acoust. Soc. Am. **132**, 789–798 (2012).
[13]T. Bravo, C. Maury, and C. Pinhède, "Sound absorption and transmission through flexible micro-perforated panels backed by an air layer and a thin plate," J. Acoust. Soc. Am. **131**, 3853–3863 (2012).
[14]T. Bravo, C. Maury, and C. Pinhède, "Enhancing sound absorption and transmission through flexible multi-layer micro-perforated structures," J. Acoust. Soc. Am. **134**, 3663–3673 (2013).
[15]C. Wang and L. Huang, "On the acoustic properties of parallel arrangement of multiple micro-perforated panel absorbers with different cavity depths," J. Acoust. Soc. Am. **130**, 208–218 (2011).
[16]X. Li, X. Yu, and W. Zhai, "Additively manufactured deformation-recoverable and broadband sound-absorbing microlattice inspired by the concept of traditional perforated panels," Adv. Mater. **33**, 2104552 (2021).
[17]X. Li, X. Yu, M. Zhao, Z. Li, Z. Wang, and W. Zhai, "Multi-level bioinspired microlattice with broadband sound-absorption capabilities and deformation-tolerant compressive response," Adv. Funct. Mater. **33**, 2210160 (2023).
[18]Z. Liu, J. Zhan, M. Fard, and J. L. Davy, "Acoustic properties of multilayer sound absorbers with a 3D printed micro-perforated panel," Appl. Acoust. **121**, 25–32 (2017).
[19]G. Catapane, G. Petrone, and O. Robin, "Series and parallel coupling of 3D printed micro-perforated panels and coiled quarter wavelength tubes," J. Acoust. Soc. Am. **154**(5), 3027–3040 (2023).
[20]T. G. Zieliński, F. Chevillotte, and E. Deckers, "Sound absorption of plates with micro-slits backed with air cavities: Analytical estimations, numerical calculations and experimental validations," Appl. Acoust. **146**, 261–279 (2019).
[21]J. Kennedy, L. Flanagan, L. Dowling, G. J. Bennett, H. Rice, and D. Trimble, "The influence of additive manufacturing processes on the performance of a periodic acoustic metamaterial," Int. J. Polym. Sci. **2019**, 7029143.
[22]Y. Qian, D. Kong, S. Liu, S. Sun, and Z. Zhao, "Investigation on micro-perforated panel absorber with ultra-micro perforations," Appl. Acoust. **74**, 931–935 (2013).
[23]W. J. Tzeng and F. Y. Wu, "Theory of impedance networks: The two-point impedance and *LC* resonances," J. Phys. A: Math. Gen. **39**, 8579–8591 (2006).
[24]F. Wu, Y. Xiao, D. Yu, H. Zhao, Y. Wang, and J. Wen, "Low-frequency sound absorption of hybrid absorber based on micro-perforated panel and coiled-up channels," Appl. Phys. Lett. **114**, 151901 (2019).
[25]H. Li, J. Wu, S. Yan, and Q. Mao, "Design and study of broadband sound absorbers with partition based on micro-perforated panel and Helmholtz resonator," Appl. Acoust. **205**, 109262 (2023).